Supporting Information

Nonvolatile Memory Properties of Sol-Gel Derived Niobium Oxide Films

Hyunhee Baek[1§], Chanwoo Lee[2§], Jungkyu Choi[1*] and Jinhan Cho[1*]

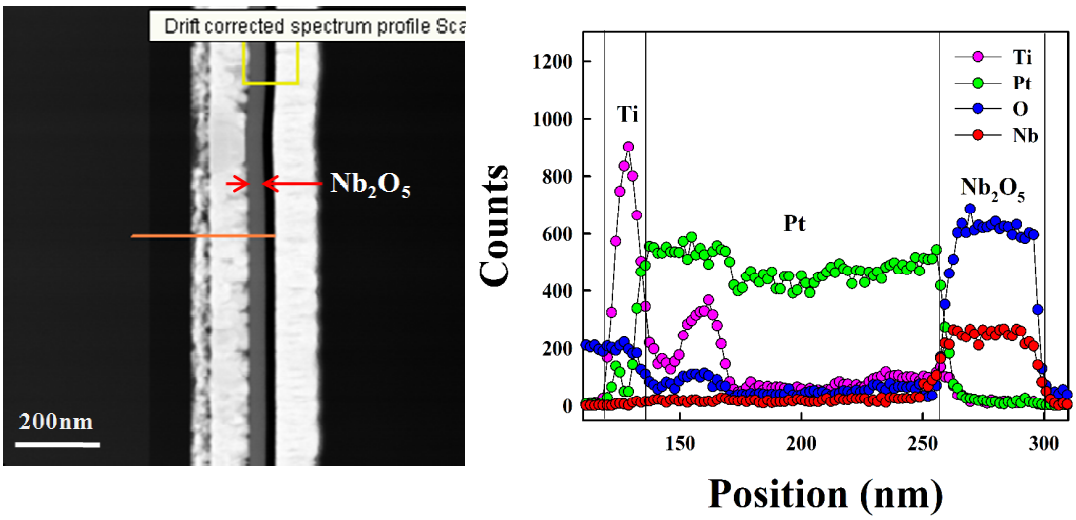

Figure S1. Depth-distribution profile of oxygen composition within Nb_2O_5 film annealed at 620 ^{o}C.

Figure S2. Electrical switching behavior of sol-gel derived Nb_2O_5 devices measured from 100 samples. About 30 samples within red lines displayed malfunctional switching behavior. As a result, our devices showed the output performance of about 70 %.

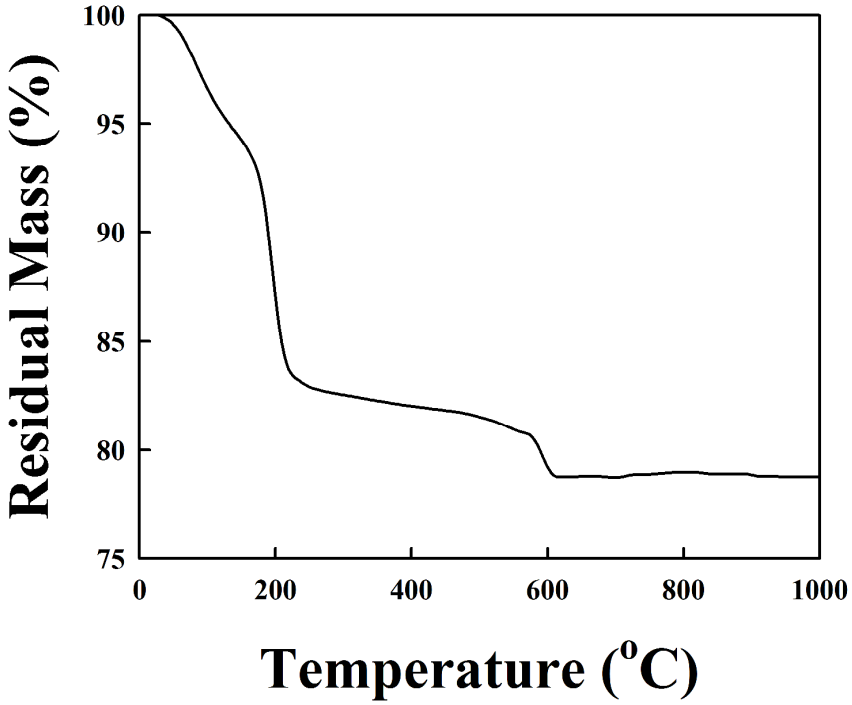

Figure S3. Thermogravimetric analysis of niobium ethoxide. The mass loss of about 23 % was observed during the formation of Nb_2O_5 films.

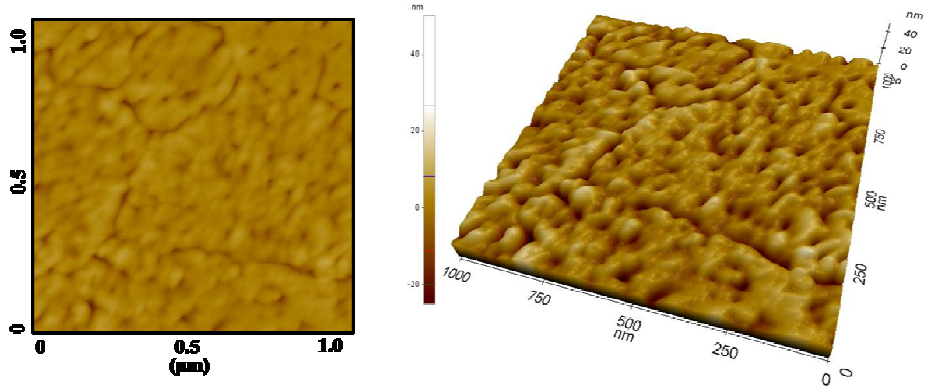

Statistics

Region	Min(nm)	Max(nm)	Mid(nm)	Mean(nm)	Rpv(nm)	Rq(nm)	Ra(nm)	Rz(nm)	Rsk	Rku
Whole	-20.049	8.257	-5.896	0.000	28.306	2.681	2.023	27.799	1.056	5.254

Figure S4. AFM image of 48 nm-thick Nb_2O_5 film with RMS surface roughness of about 2.68 nm

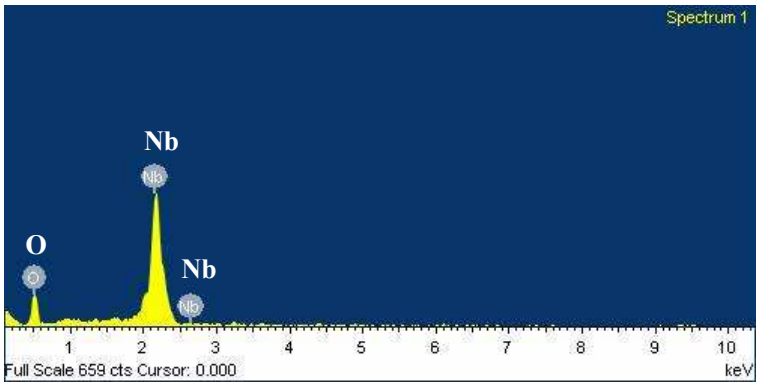

Figure S5. The EDS (Energy Dispersive Spectrometer) analysis of Nb_2O_5 film devices thermally annealed at 620 ^{o}C.

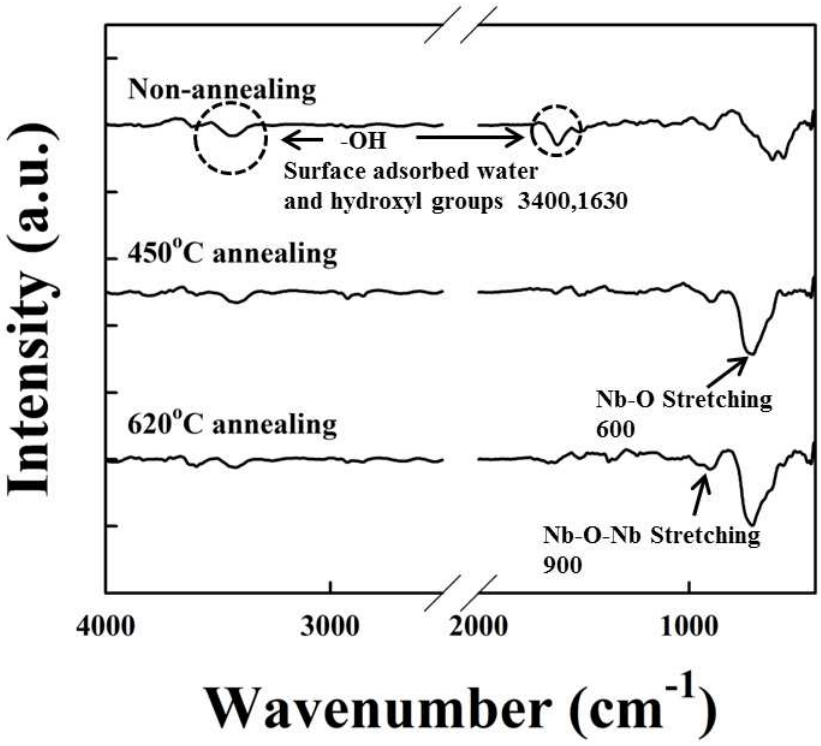

Figure S6. FT-IR spectra of $Nb(OCH_2CH_3)_5$ and Nb_2O_5 films thermally annealed at 450 and 520°C.

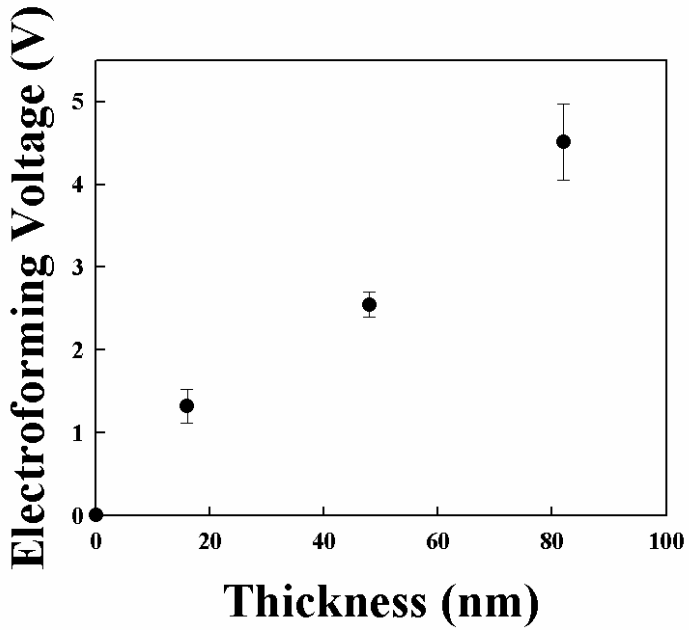

Figure S7. Electroforming voltage of sol-gel derived devices as a function of Nb_2O_5 film thickness.

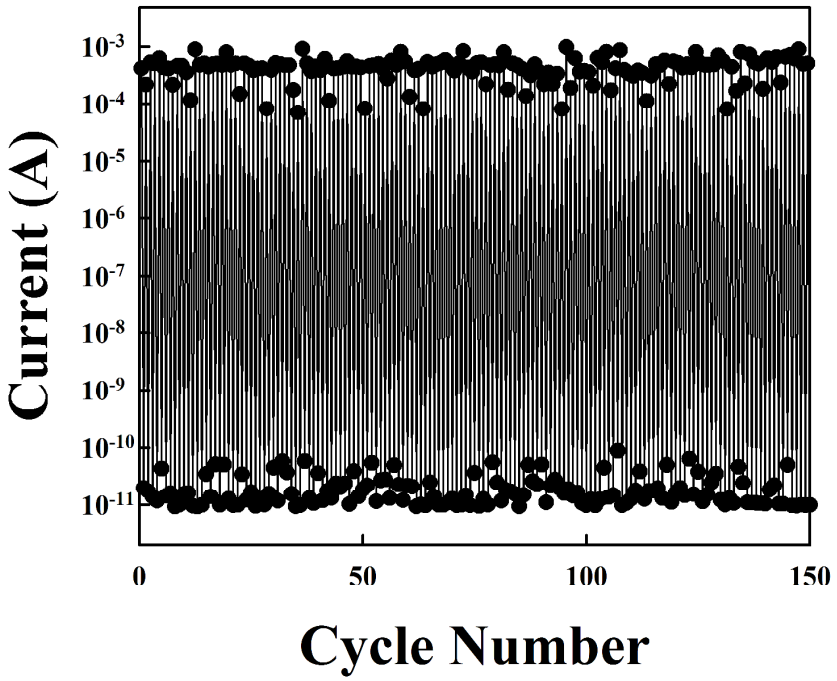

Figure S8. Cycling test of Nb_2O_5 devices measured from a switching speed of 600 μs.

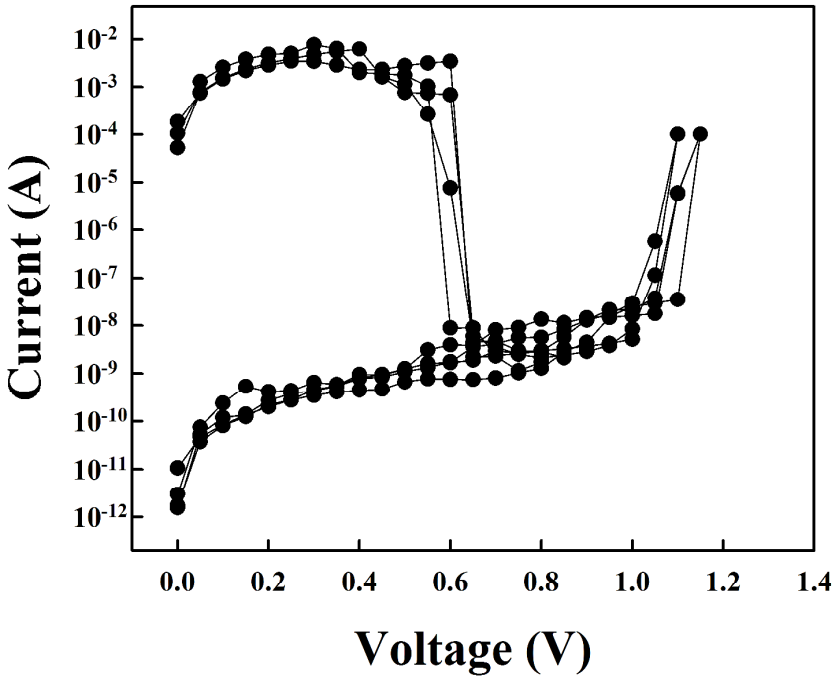

Figure S9. *I-V* curves of sol-gel derived Nb_2O_5 devices measured after one year.

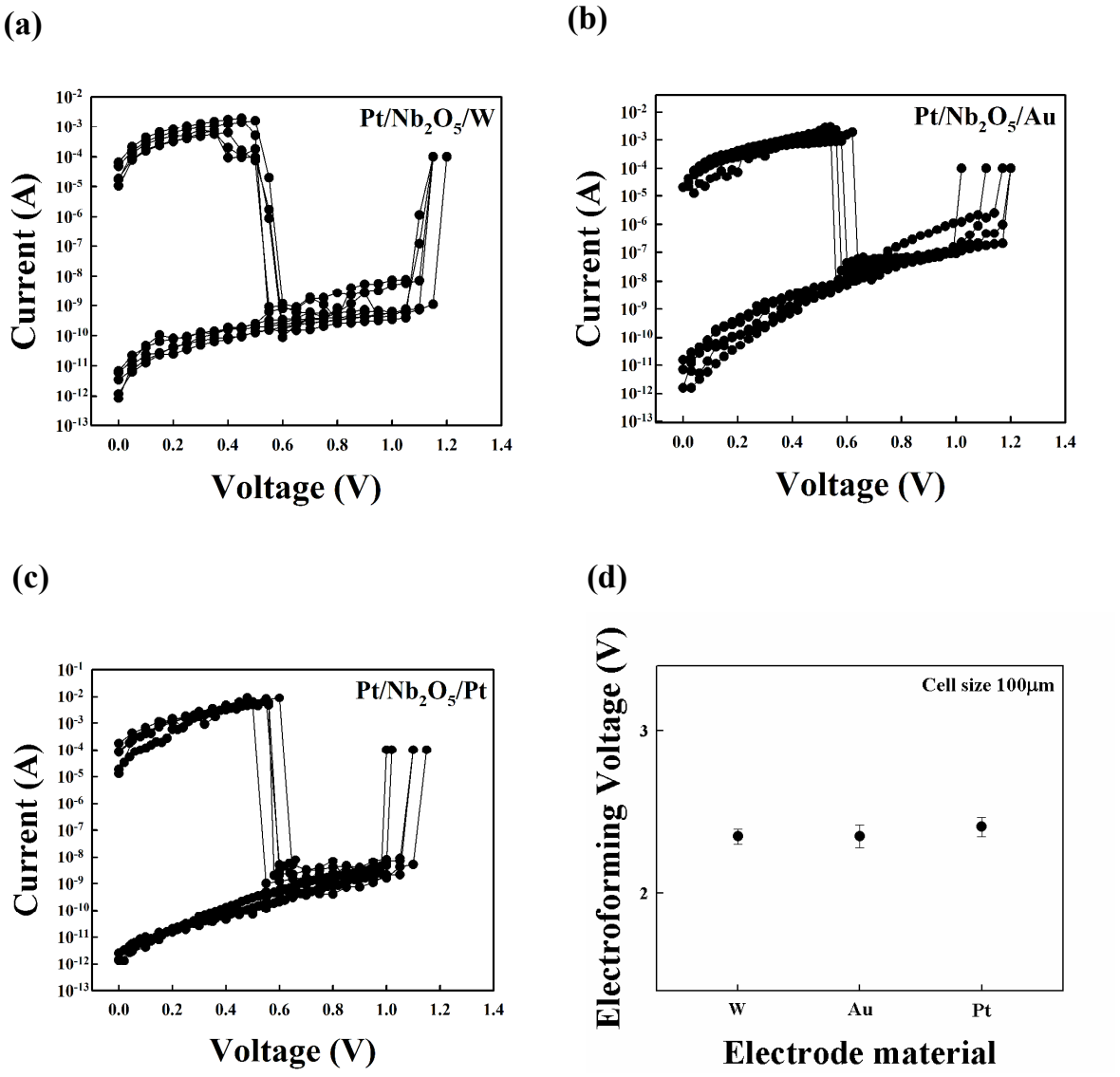

Figure S10. *I-V* curves of sol-gel derived Nb_2O_5 devices (annealed at 620 ^oC) measured from (a) W (tungsten) (b) Au (gold), and (c) Pt (platinum) top electrodes. (d) Electroforming voltages of Nb_2O_5 film devices with W, Au and Pt top electrodes.

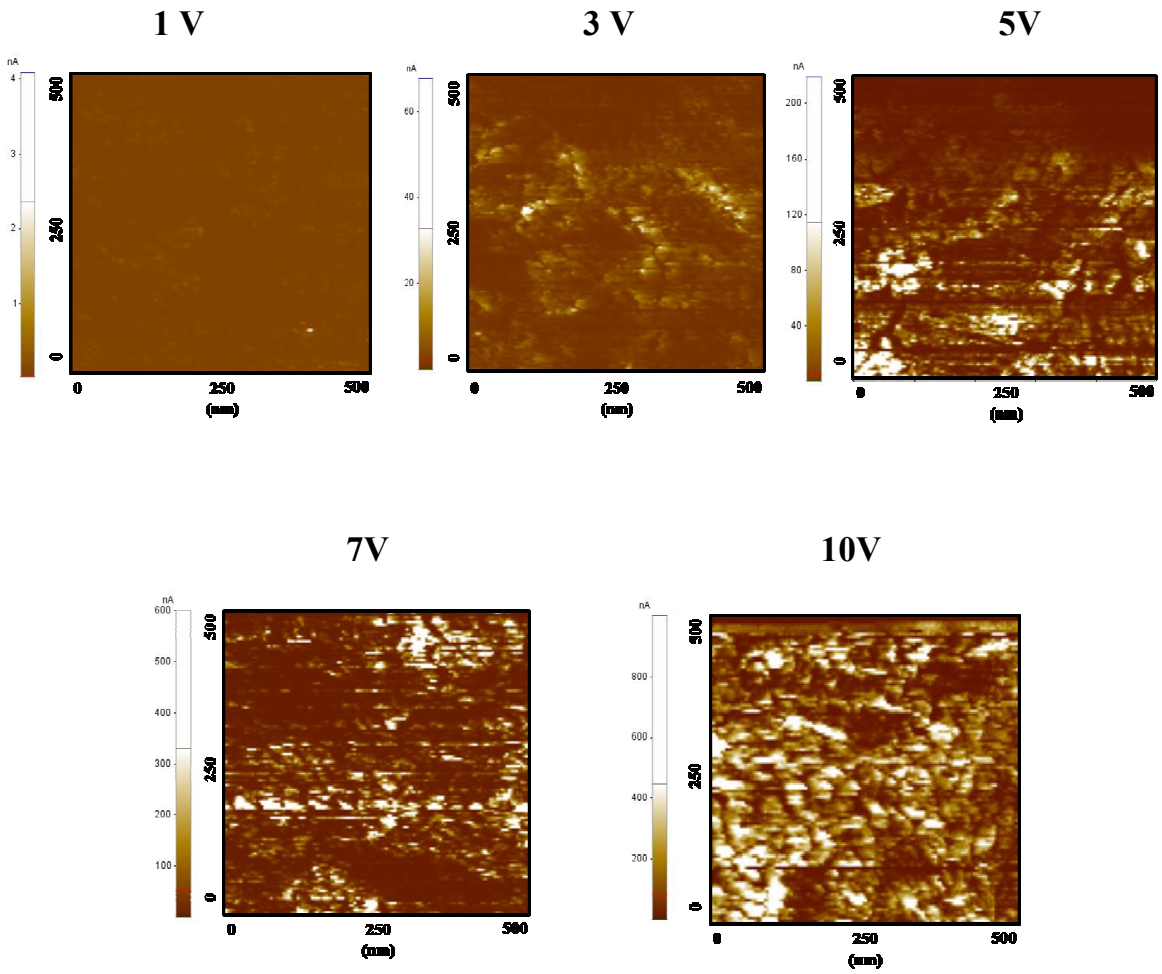

Figure S11. CS-AFM images of Nb_2O_5 films measured with increasing initial electroforming voltage from 1 to 10 V. At 10V, the films lost their reversible switching properties as a result of dielectric break down.

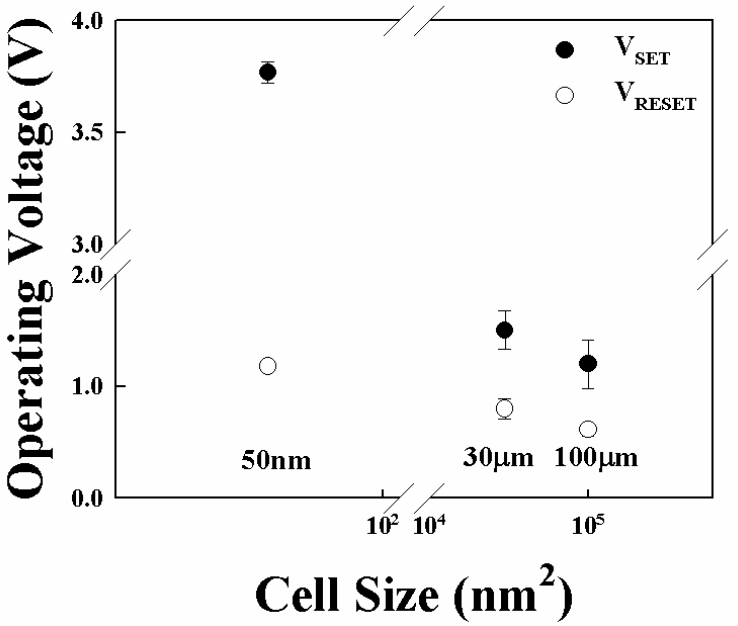

Figure S12. Cell size dependences of operating voltages of Nb_2O_5 film devices.

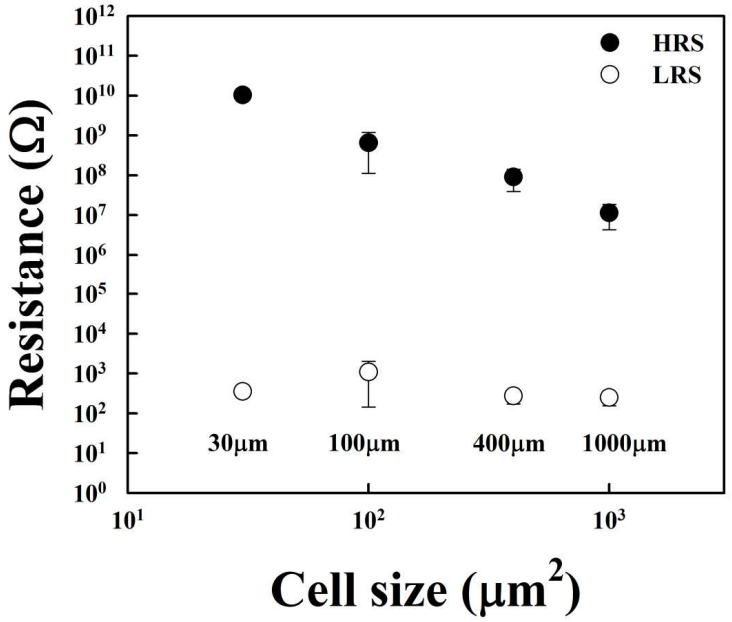

Figure S13. Dependences of resistance characteristics on a cell area for LRS and HRS.

(a)

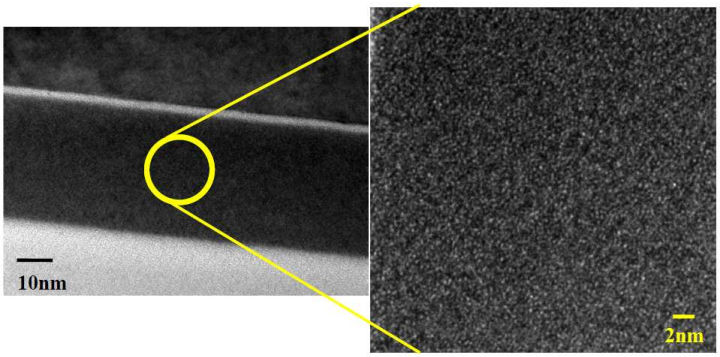

(b)

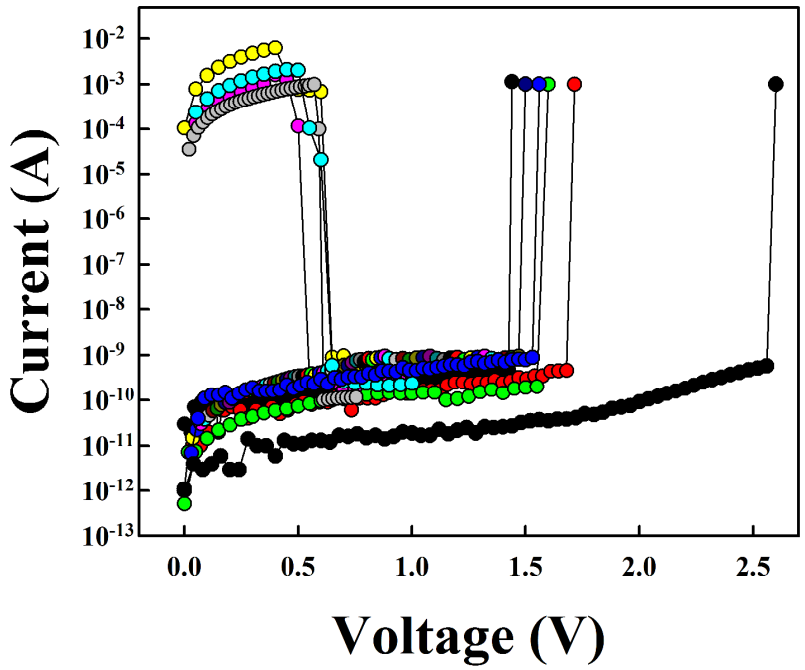

Figure S14. (a) Cross-sectional HR-TEM image of amorphous Nb_2O_5 films. (b) *I-V* curves of sol-gel derived Nb_2O_5 devices. These Nb_2O_5 films were annealed at 450 ^{o}C (2 h under nitrogen atmosphere, and furthermore 2 h under oxygen condition).

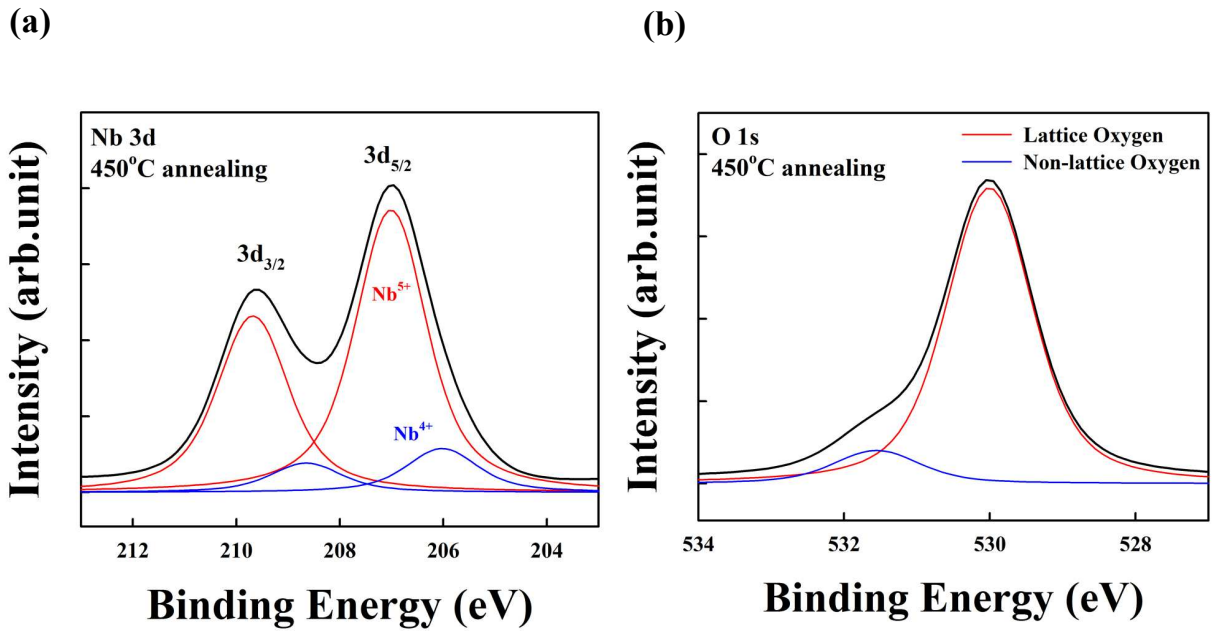

Figure S15. XPS deconvoluted spectra of (a) Nb3d and (c) O1s of Nb_2O_5 films annealed at 450 ^{o}C.

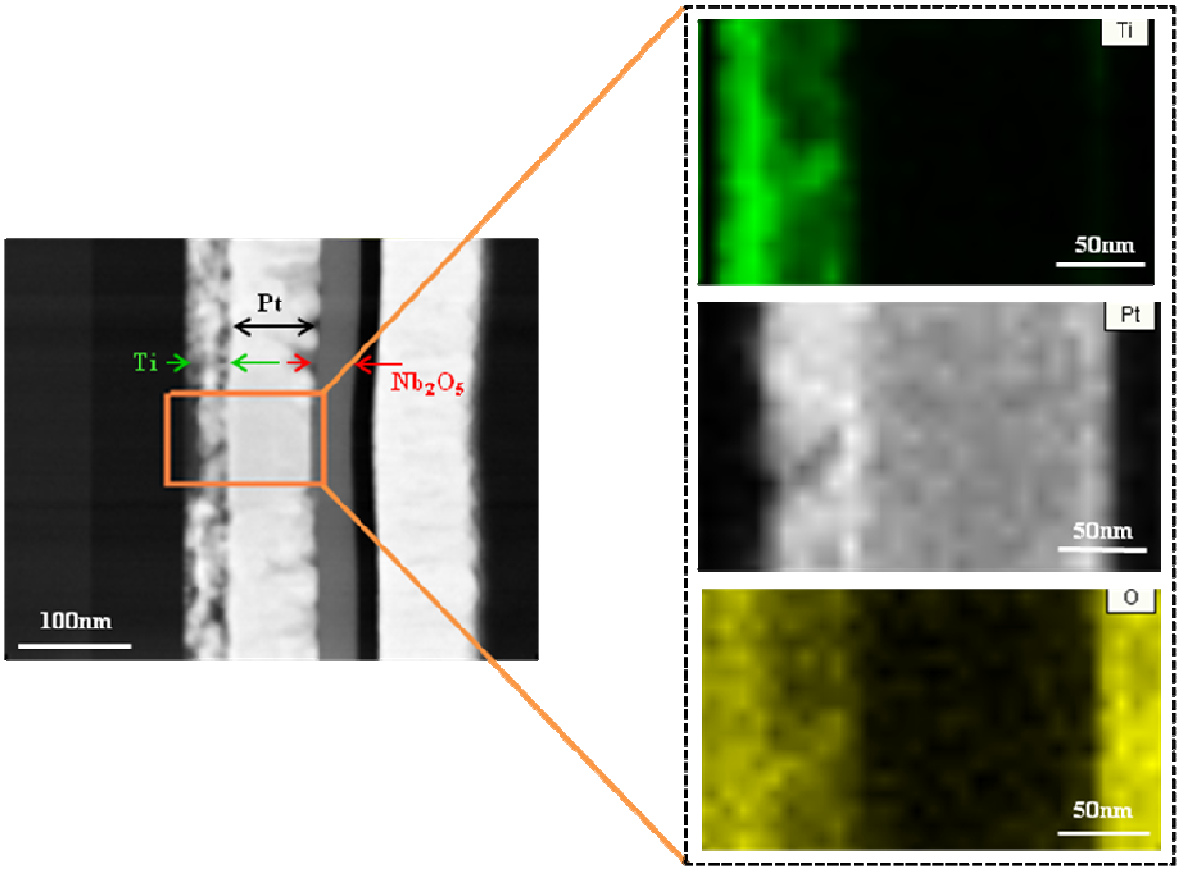

Figure S16. EF-TEM image map of Ti/Pt/Nb_2O_5 film marked by a square region.

(a)

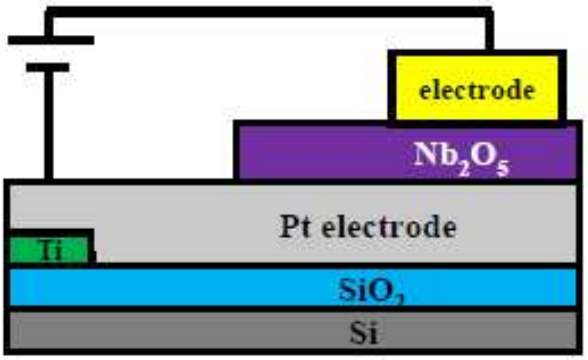

(b)

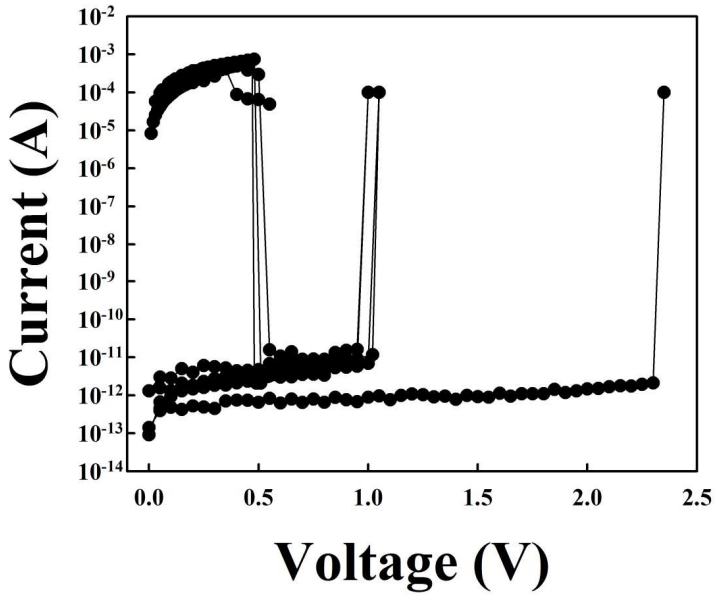

Figure S17. (a) Schematic and (b) *I-V* curves of sol-gel derived Nb_2O_5 devices without Ti layer. Nb_2O_5 films were thermally annealed at 620 ^{o}C.